Journal of Solid State Chemistry 274 (2019) 182–187

Contents lists available at ScienceDirect

Journal of Solid State Chemistry

journal homepage: www.elsevier.com/locate/jssc

Pressure induced phase transformations in diisopropylammonium bromide

Shradhanjali Sahoo [a], T.R. Ravindran [a,*], V. Srihari [b], K.K. Pandey [b], Sharat Chandra [a], C. Thirmal [c,1], P. Murugavel [c]

[a] Materials Science Group, Indira Gandhi Centre for Atomic Research, HBNI, Kalpakkam, Tamil Nadu, 603102, India
[b] High Pressure and Synchrotron Radiation Physics Division, Bhabha Atomic Research Centre, Mumbai 400085, India
[c] Department of Physics, Indian Institute of Technology, Madras, Chennai 600036, India

ARTICLE INFO

Keywords:
Molecular ferroelectric
High pressure
X-ray diffraction
Raman spectroscopy

ABSTRACT

Effect of high pressure on ferroelectric diisopropylammonium bromide (DIPAB) is investigated using Raman spectroscopy and angle-dispersive x-ray diffraction (XRD) measurements using a diamond anvil cell up to ~10 GPa. Raman spectroscopic studies indicate that the monoclinic (m-II) ferroelectric phase of DIPAB is unstable under slight compression, leading to changes in molecular conformation. We have observed new peaks appearing in the lattice mode region and CH_3 stretching region giving indication of conformational change. XRD investigations reveal that the m-II phase (space group $P2_1$) is partially transformed into a centrosymmetric, non-polar triclinic (P-1) structure at 0.7 GPa. Ferroelectricity is expected to weaken under compression above 0.7 GPa and ferroelectricity may disappear at a very high pressure when the m-II phase fully converted into triclinic P-1 phase. On releasing the pressure the ambient structure is fully recovered. The role of hydrogen bonds in the phase transformation is also discussed.

1. Introduction

Molecular organic materials are of current interest because of their multi-functionality, ease of processing, and low cost. They exhibit pressure and temperature induced polymorphism as well as conformation changes, and this affects their physical and chemical properties [1–9]. There are efforts to synthesize small molecular ferroelectrics, but there are not many with Curie temperature (T_c) above room temperature [10,11]. Recently several room temperature molecular ferroelectric materials such as croconic acid crystals, imidazolium-based molecular ferroelectrics, diisopropylammonium salts such as diisopropylammonium chloride (DIPAC), diisopropylammonium perchlorate (DIPAP) and diisopropylammonium bromide (DIPAB) [12–16] have been synthesized with Curie temperature above 300 K.

Among organic molecular ferroelectrics, diisopropylammonium bromide (DIPAB) has a high spontaneous polarization $P_s = 23\ \mu C/cm^2$ and a high dielectric constant of 85 (@400 Hz), comparable to that of $BaTiO_3$ [16]. At room temperature, DIPAB can be stabilized in either an orthorhombic (space group $P2_12_12_1$) or a monoclinic-II (m-II, $P2_1$) structure depending on synthesis conditions [16–24]. The non-polar orthorhombic structure exhibits a subtle, irreversible phase transformation to the ferroelectric m-II phase above ~417 K. At a slightly higher temperature of 426 K this m-II phase reversibly transforms into a disordered, paraelectric monoclinic I (m-I, $P2_1/m$) structure [16,17,20–23]. Another low-temperature phase transition was observed from m-II to monoclinic P21/n structure at 173 K [25].

As DIPAB has potential applications, it is important to investigate its stability under various external conditions such as high pressure and temperature. Temperature dependent phase transformations of ortho DIPAB have been explored using x-ray diffraction [16,17,20,22,23], whereas there are no reports of the effects of pressure on DIPAB and related compounds. In order to gain understanding of the high pressure structural and vibrational properties, in the present work, (i) we investigate pressure induced structural changes in the ferroelectric DIPAB phase up to 10 GPa at ambient temperature by x-ray diffraction and Raman spectroscopy; (ii) we obtain its bulk modulus from high-pressure XRD measurements and investigate possible reasons for phase transformation.

2. Experimental and computational details

DIPAB was synthesized using a solution growth technique.

---

* Corresponding author.
E-mail address: trr@igcar.gov.in (T.R. Ravindran).

[1] Present address: VNR-Vignana Jyothi Institute of Engineering and Technology, Hyderabad.

https://doi.org/10.1016/j.jssc.2019.03.025
Received 25 January 2019; Received in revised form 15 March 2019; Accepted 15 March 2019

Diisopropylamine and 48% aqueous hydrobromic acid were reacted in 1:1 M ratio, and after a few days, a transparent polycrystalline solid was formed by slow evaporation. This was recrystallized in a mixture of undistilled methanol and ethanol (1:1) at room temperature, and translucent block-shaped crystals (Phase I) were formed after ~60 days in a Petri dish [24].

Some of these crystals were ground into a fine powder in an agate mortar and pestle for 30 min; phase identification was carried out by powder x-ray diffraction technique with a diffractometer (STOE, Germany) using CuKα radiation (1.5406 Å) in the 2θ range of 7–70° with a step size of 0.05°. Part of this Phase I sample was annealed at 429 K for 15 min, and powder XRD pattern was recorded on this Phase II sample. Phase I pattern matches with that reported in the literature as the orthorhombic $P2_12_12_1$ phase, and Phase II the monoclinic-II, $P2_1$ phase [17]. There were no extra peaks in either of the samples, and the purity of these phases is established (Supplementary Figs. S1 and S2). Rietveld refined lattice parameters are obtained (Supplementary Table T1).

Raman spectroscopic measurements on m-II sample as a function of pressure up to 10 GPa at ambient temperature were recorded using a micro Raman spectrometer (Renishaw, UK, model inVia) with 514.5 nm laser excitation. Spectra in the range 20–100 cm^{-1} were recorded using a low wave number filter (called 'Eclipse filter'). The laser was focused to a spot size of ~1 μm with a 20 × microscope objective. Laser power on the sample was kept low (~2 mW) to avoid burning the samples. The resolution of the instrument is ~1.5 cm^{-1} per pixel of the CCD detector. Powder sample of m-II DIPAB was loaded along with a few ruby specks for pressure measurement in a 200 μm hole in a pre-indented stainless steel gasket mounted in a compact, symmetric diamond anvil cell with anvils of culet diameter 500 μm. No hydrostatic medium was used. Solid DIPAB dissolves in most conventional hydrostatic media, and silicone oil has several Raman bands that interfere with those of the sample.

In-situ angle dispersive x-ray diffraction experiments at high pressure were carried out on m-II samples at beamline-11 of INDUS-2 synchrotron (in RRCAT, Indore, India) [26] with a monochromatic x-rays of wavelength 1.0065(4) Å and beam dimensions 90 μm × 30 μm. The sample was ground into a fine powder in an agate mortar and loaded into a 150 μm diameter hole drilled in a tungsten gasket in a Mao Bell type diamond anvil cell (DAC) along with silicone oil medium and gold pressure marker [27]. Error in pressure determination is expected to be not more than 0.1 GPa. Error in P measurement could arise from pressure gradients across the sample chamber, and this is minimized by recording ruby luminescence spectra at the same spot where the sample spectra are recorded. Diffraction patterns were recorded using a mar345 imaging plate detector; sample to detector distance and wavelength were calibrated using standard samples of CeO_2 and LaB_6. The diffraction intensity was normalized to constant exposure time for analysis of the patterns. The two-dimensional diffraction images were azimuthally integrated using the FIT2D software [28]. Using Fullprof software we obtained lattice parameters [29]. New phases are indexed by treor90 and divol 06 program that is part of Expo 2014 package [30–32]. We have used 'Powder cell' to visualize the possible Bragg positions in new structures [33].

First principles calculations were carried out using DFT based $Dmol^3$ code in the Material Studio version 6.0 (Accelrys) [34] package. Geometry optimization involves minimizing the magnitude of the calculated forces and stresses until they become smaller than convergence tolerances. The general gradient approximation (GGA) with Perdew–Burke–Ernzerhof (PBE) [35] as the exchange correlation functional, DNP numerical basis set and the program option fine grid size (0.04 $Å^{-1}$) was employed in the calculation. The initial structures were adopted from experimentally reported crystal structures in the Cambridge Crystallographic Data Centre (CCDC) for diisopropyl ammonium bromide: m-II (CCDC-893211) [17]. During relaxation process, the total energy of the system was converged to less than 2×10^{-5} eV, the residual forces less than 0.002 Ha/Å, the displacement of the atoms less than 0.002 Å. K-point sampling for m-II phase was 4 × 4 × 4. Here we have adopted density functional calculations to assign external modes which were not discussed explicitly.

Table 1
Assignment of intermolecular modes obtained from $Dmol^3$.

Mode No.	Expt. m-II wavenumber (cm^{-1})	GGA/PBE $DMol^3$ wavenumber (cm^{-1})	Ref. [24] wavenumber (cm^{-1})	Mode assignments
1	38	46	42	Out of phase cation lib. + anion Trans.
2	47	50	52	CH_3 lib.
3	54	56	61	In phase cation + anion lib.
4	75	77	73	Out of phase propyl lib.
5	–	–	87	Out of phase propyl lib.
6	97	99	104	Out of phase cation lib.
7	112	108	109	Out of phase cation lib.

Note: lib.-Libration; cation-diisopropyl ammonium cation; anion-bromine ion; trans.-Translation; Expt.-Experiment.

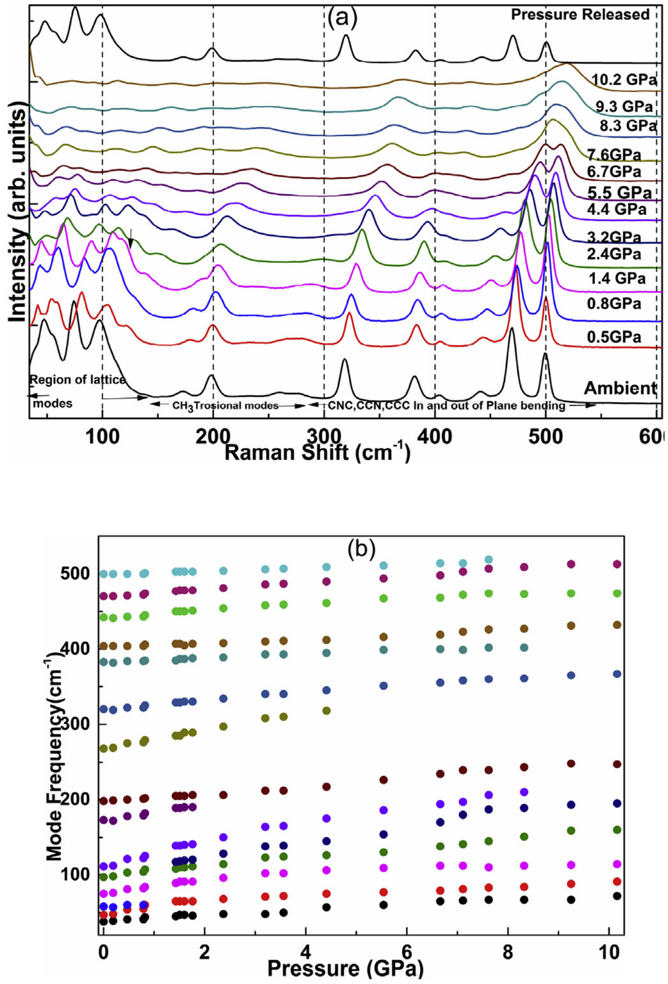

Fig. 1. (a) Raman spectra of m-II DIPAB in the spectral region 30- 700 cm-1 as a function of pressure (b) Mode frequency versus pressure of Raman modes in the spectral region 30- 700 cm-1.

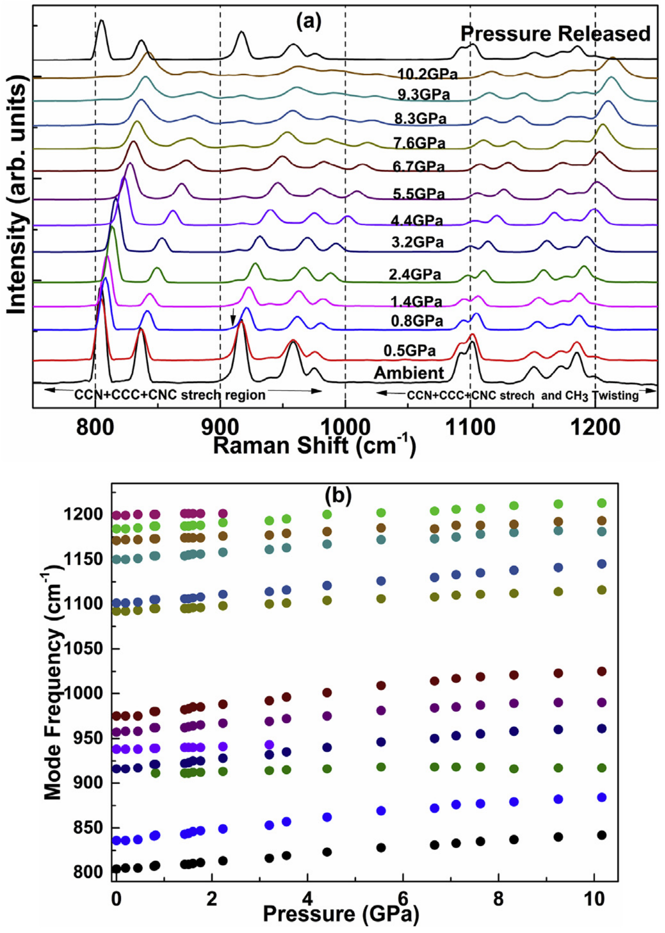

Fig. 2. **(a)** Raman spectra of m-II DIPAB in the spectral region 700- 1260 cm^{-1} as a function of pressure; **(b)** Mode frequency versus pressure in this spectral region.

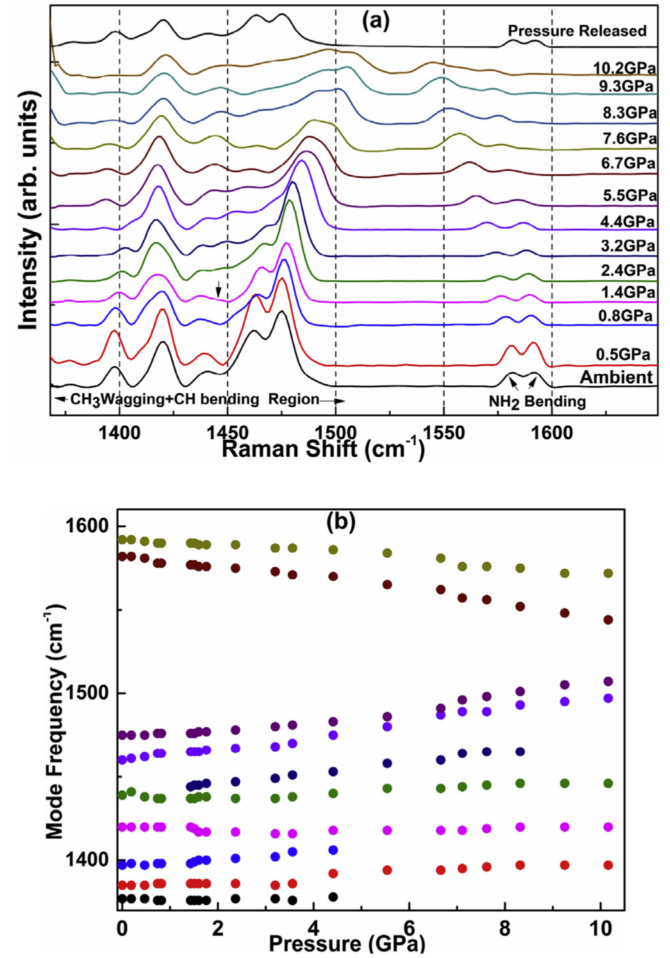

Fig. 3. **(a)** Raman spectra of m-II DIPAB in the spectral region 1360- 1650 cm^{-1} as a function of pressure; **(b)** Mode frequency versus pressure in the spectral region 1360-1650 cm^{-1}.

3. Results and discussion

The orthorhombic polymorph of DIPAB has four molecules per unit cell, and the structure is composed of hydrogen-bonded zigzag chains. Each diisopropylammonium cation is bonded to two neighboring bromide anions by hydrogen bonds [17]. The ferroelectric m-II ($P2_1$) structure has two molecules per unit cell.

For the m-II phase, factor group analysis using correlation method results in the following phonon irreducible representation [24].

$$\Gamma_{\text{Optical}} = 70\text{A} + 71\text{B}\ (141\ \text{optical modes})$$

$$\Gamma_{\text{Acoustic}} = \text{A} + 2\text{B}$$

All these optical modes are Raman active, though experimentally we obtain only 52 Raman bands [24]. In the case of molecular solids such as DIPAB, the intermolecular interactions are weak compared to intramolecular interactions. If we consider a single diisopropylammonium bromide unit, group theory predicts a much smaller number of 66 Raman bands that is close to the experimental results [24]. Assignment of intermolecular modes obtained from Dmol^3 calculations are given below (Table 1).

3.1. *High-pressure Raman spectroscopic studies on DIPAB m-II phase*

Below 150 cm^{-1} the m-II phase has Raman bands at 38, 47, 54, 75, 97 and 112 cm^{-1} and a shoulder at 38 cm^{-1}. All bands in this region show normal blue shift under compression. At 1.4 GPa, a new peak marked by an arrow (Fig. 1) emerges at 117 cm^{-1} which appears as a shoulder of the ambient band at 96 cm^{-1}. This shoulder becomes a distinct peak at higher pressures. The 38 cm^{-1} band which is a shoulder at ambient conditions gains intensity in the high-pressure region and evolves into an intense band at 1.4 GPa. No other new band appears in the region 160-700 cm^{-1} up to 10 GPa. All wavenumbers increase monotonically with pressure.

Low energy lattice modes are sensitive to the crystal structure, and any change or appearance of new modes in this region can be directly correlated to a structural phase transition. There are several reports on molecular solids where high-pressure phase transition has been detected by observing changes in the low-frequency modes [1,3–5,36,37]. Spectral changes in lattice modes at 1.4 GPa indicate the possibility of a phase transition at this pressure.

In the region 700-1260 cm^{-1} bands arise from CCC, CNC, and CCN stretching, CH_3 twisting vibrations [24]; a new band appears at 0.8 GPa around 912 cm^{-1} near CNC antisymmetric stretch mode at 916 cm^{-1}, and it gains intensity at higher pressures (Fig. 2a).

In the range 1360–1600 cm^{-1} the bands correspond to CH_3 wag, CH_3 twist, and NH_2 bending motions [24]. Here we observe two kinds of behavior: the bands at 1375, 1397, 1410, 1421, 1439 and 1475 cm^{-1} exhibit normal blue shift whereas the NH_2 bending modes at 1582 and 1592 cm^{-1} show a red shift under compression. The latter signifies an elongation of N—H bonds and contraction of the H...Br distance indicating the formation of stronger hydrogen bonds. Similar red shift is observed in the N—H stretching mode at 3163 cm^{-1}. At 1.4 GPa a new

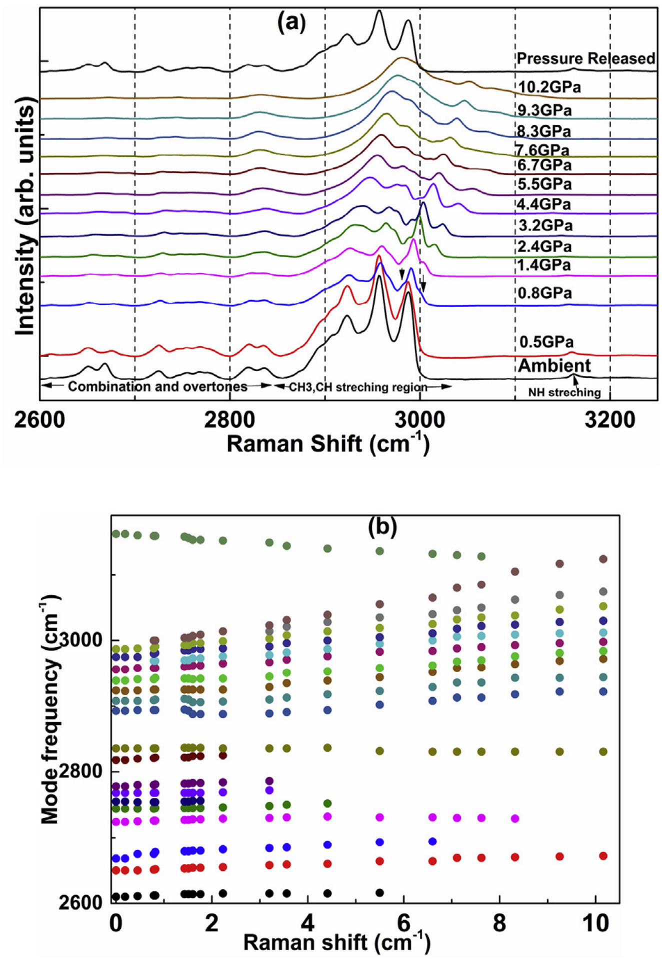

Fig. 4. **(a)** Raman spectra of DIPAB in the spectral region 2700-3500 cm^{-1} as a function of pressure; **(b)** Mode frequency versus pressure in this spectral region.

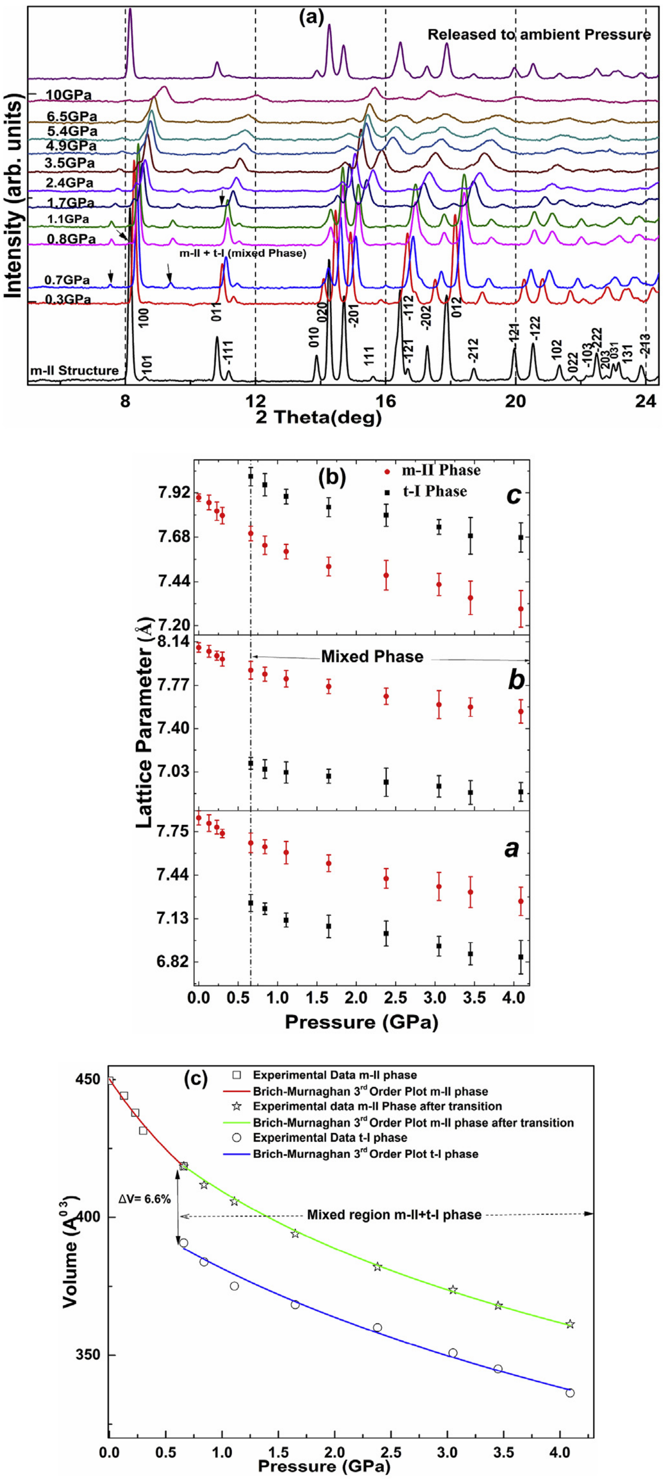

Fig. 5. **(a)** High-pressure x-ray diffraction plot of DIPAB m-II phase at several different pressures. Arrows in the plot indicate new peaks at that pressure **(b)** Pressure verses lattice parameter plot before phase transition m-II phase and after transition t-I phase; with corresponding error values of lattice parameter **(c)** Pressure versus volume change before and after phase transition and Birch-Murnaghan 3rd order equation plot for m-II and t-I phase.

band appears at 1449 cm^{-1} in the CH_3 wag region (marked by an arrow in Fig. 3a).

Stretching modes of CH, CH_3, combination and overtone bands are observed in the spectral range 2700–3500 cm^{-1} [24]. The new bands emerging at 2969 and 3000 cm^{-1} in the CH_3 stretching region (marked by arrows in Fig. 4a and (b)) at 0.8 GPa suggest possible conformal changes in the cation in this pressure range. A similar observation was made in the case of L-isoleucine crystals [36]. Except for the NH stretching mode at 3163 cm^{-1}, all bands blue shift with pressure (Figs. 3a and 4(a)). Mode Grüneisen parameters are obtained for all the modes which is defined as $\gamma_{i0} = \frac{K_{T0}}{\nu_{i0}} \left(\frac{\partial \nu_i}{\partial P} \right)_0 = -\left(\frac{\partial \ln \nu_i}{\partial \ln V}\right)_0$ [38]; where ν_i is the frequency of the ith mode, V is the volume, P is the pressure and K_{T0} is the bulk modulus. The modes associated with N—H stretching modes have negative Grüneisen parameters; rest of the modes are positive (supplementary Table T2).

As pressure is increased, there is a red shift in the NH_2 bending and N—H stretching bands, indicating that the N—H distance increases and the H…Br hydrogen bond is getting stronger. Inter-molecular as well as intramolecular distances in the DIPAB molecules decrease. Reduction of H…Br distance, Br^- anion mobility is likely to affect the cation, leading to a conformation change. This conformation change and stronger hydrogen bond network gives rise to new modes in the lattice mode region of the m-II phase at 0.7 GPa. So these structural transitions are due to a conformation change and a modified hydrogen network. There are reports of conformational changes leading to a modification of the arrangement of molecules and ultimately it has been observed as a structural change in the crystals [36,37,39–42]. Non-hydrostatic nature of pressure transmitting media at high pressure can affect the phase transition pressure. Silicone oil is hydrostatic up to ~ 5 GPa. Since the phase transition from m-II to t-I of DIPAB occurs at a low pressure of 0.7 GPa the pressure transmitting medium of silicone oil is not expected to affect the transition pressure [43,44]. To confirm the structural

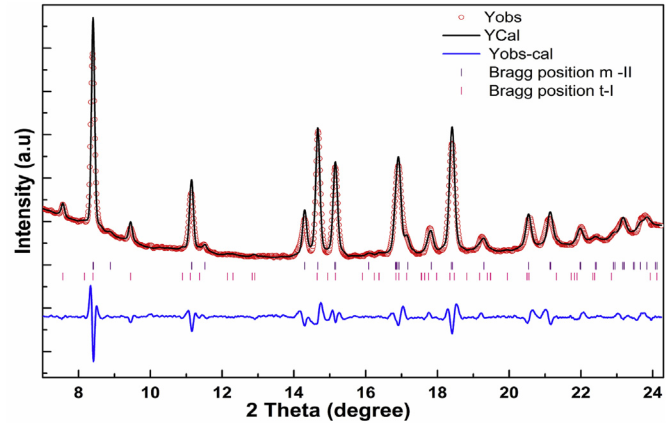

Fig. 6. Two phase Le Bail fitting for m-II phase and new t-I phase at 1.7 GPa.

Table 2
Fitted parameters obtained from Le-Bail fitting.

Fitted parameters	m-II phase	t-I phase
R_P	6.2	9.1
R_{WP}	7.5	8.3
R_{Exp}	8.8	9.8

changes, we have carried out X-Ray diffraction measurements on the sample, and the results are discussed in the next Section.

3.2. *High-pressure X-Ray diffraction studies on ferroelectric DIPAB*

Under compression all peaks shift towards higher 2θ values indicating a decrease of *d* spacing in DIPAB. Lattice parameters are refined using Fullprof software. Three new peaks at 7.3°, 8.1° and 9.4° (Fig. 5a, marked with arrows) appear at 0.7 GPa, and one more at 10.8° at 1.7 GPa indicting emergence of a new phase at this pressure. To index the new phase at this pressure we used Treor, and divol 06 programs. During initial indexing we considered all the peaks including new ones; we obtained two possible space groups one of which is monoclinic P2 and the other triclinic P-1 with similar lattice parameters and angles. The parent phase is $P2_1$ monoclinic that has 2 molecules per unit cell. $P2_1$ has a twofold rotation followed by a half translation. Among the possible new structures monoclinic P2 group has only one 2 fold rotation which means the number of molecules has to be doubled, which is not possible according to space group rules [45]. Triclinic P-1 space group has a one to one correspondence to $P2_1$ space group. Here we observe that new peaks appear near the parent phase's prominent peaks 100 and 011. During indexing we noted that in t-I phase all the new and some old peaks from m-II phase are present. From Fig. 5a it is clear that the parent phase exists at high pressures along with new phase t-I.

The new phase has space group P(-1) (t-I phase) with cell parameters $a = 7.241$ Å, $b = 7.102$ Å and $c = 8.009$ Å, $\alpha = 90.73$, $\beta = 107.493^\circ$ $\gamma = 90.318^\circ$, at 0.7 GPa. There is coexistence of the parent m-II phase and the new phase t-I above 0.7 GPa. We have obtained the lattice parameters for both phases up to 4 GPa [Fig. 5b]. Above this pressure the peaks become broad at higher 2theta values. Le Bail fitting of both m-II and t-I phase at 1.4 GPa is given in Fig. 6 and Table 2. The high pressure phase transition is reversible from 10 GPa [Fig. 5a], but it is possible that it would become irreversible if taken to higher pressures. To understand the behavior of lattice parameters in the m-II phase we carried out linear fits of the form $a_0 + a_1 P$ for *a, b* and *c* values. The obtained a_1 values for *a, b* and *c* are -0.344 ± 0.014 Å/GPa, -0.30 ± 0.01 Å/GPa and -0.28 ± 0.016 Å/GPa respectively. Compression is higher in the '*a*' direction compared to the '*b*' and '*c*' directions. Bulk modulus for both phases are obtained by fitting the PV curve to the 3rd order Brich-Murnaghan equation of state [46] by fixing the first derivative of bulk modulus at $B'_0 = 4$. Bulk modulus of m-II phase before transition is 7.3(8) GPa and after transition 10.1(9) whereas for t-I phase (in the mixed region) it is found to be 13.9(1.2) GPa (Table 3). Molecular organic solids generally possess bulk modulus values less than 30 GPa [47]. The bulk modulus of DIPAB is comparable to those of some recently reported porous flexible MOFs such as glycyl-L-tyrosine ($B_0 = 21.9(9)$), NH_2-MIL-53(In)($B_0 = 10.9$), ZIF-4-I ($B_0 = 16.5(5)$), and ZIF-zni($B_0 = 14$) [47–49]. The B_0 of the m = II phase of DIPAB ($B_0 = 7.3$) is close to the value of 6.5 GPa reported for fcc argon, a van der waals solid [50].

Table 3
Comparison of Bulk modulus (B_0) and its pressure-derivative (B_0') determined from Brich- Murnaghan EOS.

DIPAB Birch-Murnaghan plot	B_0(GPa)
m-II phase	7.3(8)
m-II phase after transition	10.1(9)
t-I phase	13.9(1.2)

4. Conclusions

High-pressure Raman spectroscopic study of the ferroelectric m-II phase revealed new Raman bands between 0.7 GPa in the intramolecular region, signifying a conformation change in the molecule. There are also new modes observed in the lattice mode region for m-II phase at 1.4 which indicates a structural transformation. Phase transformation is confirmed by high-pressure x-ray diffraction measurements. The high-pressure phase is indexed to a triclinic space group P-1 with cell parameters $a = 7.241$ Å, $b = 7.102$ Å and $c = 8.009$ Å, $\alpha = 90.73$, $\beta = 107.493^\circ$ $\gamma = 90.318^\circ$, at 0.7 GPa. There is a co-existence of the new and the old phases. Since the triclinic P-1 phase is centro symmetric, we expect the spontaneous polarization to reduce as pressure is increased above 0.7 GPa, and ferroelectricity may disappear at a higher pressure when the m-II phase fully converted into triclinic P-1 phase. Bulk modulus value before the phase transition is 7.3±0.82 GPa. Structural transition is due to conformation change in the molecule and distortion in the hydrogen network which was confirmed by the redshift of NH_2 bending and stretching modes.

Conflicts of interest

There are no conflicts of interest to declare.

Acknowledgements

We thank Dr. R. Rajaraman for help with Raman spectroscopic measurements, Dr. N. V. Chandra Shekar, Head, Condensed Matter Physics Division and Dr. G. Amarendra, Director, Materials Science Group for support and encouragement. Shradhanjali Sahoo thanks Homi Bhabha National Institute for Senior Research Fellowship.

Appendix A. Supplementary data

Supplementary data to this article can be found online at https://doi.org/10.1016/j.jssc.2019.03.025.

References

[1] E.V. Boldyreva, High-pressure diffraction studies of molecular organic solids. A personal view, Acta Crystallogr. Sect. A Found. Crystallogr. 64 (2008) 218–231, https://doi.org/10.1107/S0108767307065786.

[2] A. Nangia, Conformational polymorphism in organic crystals, Acc. Chem. Res. 41 (2008) 595–604, https://doi.org/10.1021/ar700203k.

[3] A. Banerji, S.K. Deb, Raman scattering study of high-pressure phase transition in thiourea, J. Phys. Chem. B 111 (2007), https://doi.org/10.1021/jp072604w, 10915–9.

[4] F.P.A. Fabbiani, C.R. Pulham, High-pressure studies of pharmaceutical compounds and energetic materials, Chem. Soc. Rev. 35 (2006) 932, https://doi.org/10.1039/b517780b.

[5] E.V. Boldyreva, High-pressure studies of the hydrogen bond networks in molecular crystals, J. Mol. Struct. 700 (2004) 151–155, https://doi.org/10.1016/j.molstruc.2004.03.026.

[6] E.V. Boldyreva, High-pressure studies of the anisotropy of structural distortion of molecular crystals, J. Mol. Struct. 647 (2003) 159–179, https://doi.org/10.1016/S0022-2860(02)00520-3.

[7] K. Gesi, Effect of hydrostatic pressure on ferroelectric and related phase transitions, Phase Transitions 40 (1992) 187–215, https://doi.org/10.1080/01411599208207747.

[8] A. Katrusiak, High-pressure X-ray diffraction studies on organic crystals, Cryst. Res. Technol. 26 (1991) 523–531, https://doi.org/10.1002/crat.2170260502.

[9] S.H. Moon, H.G. Drickamer, Effect of pressure on hydrogen bonds on organic solids, J. Chem. Phys. 61 (1974) 48–54, https://doi.org/10.1063/1.1681669.

[10] M.E. Lines, A.M. Glass, Principles and Applications of Ferroelectrics and Related Materials, Oxford University Press, 2001, https://doi.org/10.1093/acprof:oso/9780198507789.001.0001.

[11] S. Horiuchi, Y. Tokura, Organic ferroelectrics, Nat. Mater. 7 (2008) 357–366, https://doi.org/10.1038/nmat2137.

[12] Z. Pająk, P. Czarnecki, B. Szafrańska, H. Małuszyńska, Z. Fojud, Ferroelectric ordering in imidazolium perchlorate, J. Chem. Phys. 124 (2006) 144502, https://doi.org/10.1063/1.2185098.

[13] S. Horiuchi, Y. Tokunaga, G. Giovannetti, S. Picozzi, H. Itoh, R. Shimano, R. Kumai, Y. Tokura, Above-room-temperature ferroelectricity in a single-component molecular crystal, Nature 463 (2010) 789–792, https://doi.org/10.1038/nature08731.

[14] D.-W. Fu, W. Zhang, H.-L. Cai, J.-Z. Ge, Y. Zhang, R.-G. Xiong, Diisopropylammonium chloride: a ferroelectric organic salt with a high phase transition temperature and practical utilization level of spontaneous polarization, Adv. Mater. 23 (2011) 5658–5662, https://doi.org/10.1002/adma.201102938.

[15] K. Gao, M. Gu, X. Qiu, X.N. Ying, H.-Y. Ye, Y. Zhang, J. Sun, X. Meng, F.M. Zhang, D. Wu, H.-L. Cai, X.S. Wu, Above-room-temperature molecular ferroelectric and fast switchable dielectric of diisopropylammonium perchlorate, J. Mater. Chem. C. 2 (2014) 9957–9963, https://doi.org/10.1039/C4TC01882F.

[16] D.-W. Fu, H.-L. Cai, Y. Liu, Q. Ye, W. Zhang, Y. Zhang, X.-Y. Chen, G. Giovannetti, M. Capone, J. Li, R.-G. Xiong, Diisopropylammonium bromide is a high-temperature molecular ferroelectric crystal, Science (80-.) 339 (2013) 425–428, https://doi.org/10.1126/science.1229675.

[17] A. Piecha, A. Gągor, R. Jakubas, P. Szklarz, Room-temperature ferroelectricity in diisopropylammonium bromide, CrystEngComm 15 (2013) 940–944, https://doi.org/10.1039/C2CE26580J.

[18] J. Przeslawski, Z. Czapla, Linear birefringence in diisopropylammonium bromide crystal, Ferroelectrics 462 (2014) 70–73, https://doi.org/10.1080/00150193.2014.890878.

[19] C. Thirmal, P. Murugavel, V. Subramanian, Impedance spectroscopic analysis of the organic ferroelectric - diisopropylammonium bromide (DIPAB), Curr. Appl. Phys. 14 (2014) 688–690, https://doi.org/10.1016/j.cap.2014.02.018.

[20] K. Gao, C. Liu, Z. Cui, J. Zhu, H.-L. Cai, X.S. Wu, Room-temperature growth of ferroelectric diisopropylammonium bromide with 12-crown-4 addition, CrystEngComm 17 (2015) 2429–2432, https://doi.org/10.1039/C4CE02567A.

[21] K. Gao, C. Xu, Z. Cui, C. Liu, L. Gao, C. Li, D. Wu, H.-L. Cai, X.S. Wu, The growth mechanism and ferroelectric domains of diisopropylammonium bromide films synthesized via 12-crown-4 addition at room temperature, Phys. Chem. Chem. Phys. 18 (2016) 7626–7631, https://doi.org/10.1039/C6CP00568C.

[22] C. Jiang, H. Lin, C. Luo, Y. Zhang, J. Yang, H. Peng, C.G. Duan, Crystal growth and dynamic ferroelectric hysteresis scaling behavior of molecular ferroelectric diisopropylammonium bromide, J. Cryst. Growth 438 (2016) 25–30, https://doi.org/10.1016/j.jcrysgro.2015.12.019.

[23] H. Yadav, N. Sinha, S. Goel, A. Hussain, B. Kumar, Growth and structural and physical properties of diisopropylammonium bromide molecular single crystals, J. Appl. Crystallogr. 49 (2016) 2053–2062, https://doi.org/10.1107/S1600576716014552.

[24] S. Sahoo, T.R. Ravindran, S. Chandra, R.M. Sarguna, B.K. Das, T.N. Sairam, V. Sivasubramanian, C. Thirmal, P. Murugavel, Vibrational spectroscopic and computational studies on diisopropylammonium bromide, Spectrochim. Acta Part A Mol. Biomol. Spectrosc. 184 (2017) 211–219, https://doi.org/10.1016/j.saa.2017.05.006.

[25] M. Haberecht, H.W. Lerner, M. Bolte, The low-temperature phase of diisopropylammonium bromide, Acta Crystallogr. Sect. C Cryst. Struct. Commun. 58 (2002) o555–o557, https://doi.org/10.1107/S0108270102013379.

[26] K.K. Pandey, H.K. Poswal, A.K. Mishra, A. Dwivedi, R. Vasanthi, N. Garg, S.M. Sharma, Energy-dispersive X-ray diffraction beamline at Indus-2 synchrotron source, Pramana 80 (2013) 607–619, https://doi.org/10.1007/s12043-012-0493-0.

[27] D.L. Heinz, R. Jeanloz, The equation of state of the gold calibration standard, J. Appl. Phys. 55 (1984) 885–893, https://doi.org/10.1063/1.333139.

[28] A.P. Hammersley, S.O. Svensson, M. Hanfland, A.N. Fitch, D. Hausermann, Two-dimensional detector software: from real detector to idealised image or two-theta scan, High Press. Res. 14 (1996) 235–248, https://doi.org/10.1080/08957959608201408.

[29] D.B. Wiles, R.A. Young, IUCr, A new computer program for Rietveld analysis of X-ray powder diffraction patterns, J. Appl. Crystallogr. 14 (1981) 149–151, https://doi.org/10.1107/S0021889881008996.

[30] A. Altomare, C. Cuocci, C. Giacovazzo, A. Moliterni, R. Rizzi, N. Corriero, A. Falcicchio, EXPO2013 : a kit of tools for phasing crystal structures from powder data, J. Appl. Crystallogr. 46 (2013) 1231–1235, https://doi.org/10.1107/S0021889813013113.

[31] A. Altomare, C. Giacovazzo, A. Guagliardi, A.G.G. Moliterni, R. Rizzi, P.-E. Werner, New techniques for indexing: N-TREOR in EXPO, J. Appl. Crystallogr. 33 (2000) 1180–1186, https://doi.org/10.1107/S0021889800006427.

[32] A. Boultif, D. Louër, Powder pattern indexing with the dichotomy method, J. Appl. Crystallogr. 37 (2004) 724–731, https://doi.org/10.1107/S0021889804014876.

[33] W. Kraus, G. Nolze, POWDER CELL – a program for the representation and manipulation of crystal structures and calculation of the resulting X-ray powder patterns, J. Appl. Crystallogr. 29 (1996) 301–303, https://doi.org/10.1107/S0021889895014920.

[34] B. Delley, From molecules to solids with the DMol3 approach, J. Chem. Phys. 113 (2000) 7756–7764, https://doi.org/10.1063/1.1316015.

[35] J.P. Perdew, K. Burke, M. Ernzerhof, Generalized gradient approximation made simple, Phys. Rev. Lett. 77 (1996) 3865–3868, https://doi.org/10.1103/PhysRevLett.77.3865.

[36] A.S. Sabino, G.P. De Sousa, C. Luz-Lima, P.T.C. Freire, F.E.A. Melo, J. Mendes Filho, High-pressure Raman spectra of L-isoleucine crystals, Solid State Commun. 149 (2009) 1553–1556, https://doi.org/10.1016/j.ssc.2009.05.048.

[37] P.F. Façanha Filho, P.T.C. Freire, F.E.A. Melo, V. Lemos, J. Mendes Filho, P.S. Pizani, D.Z. Rossatto, Pressure-induced phase transitions in L-leucine crystal, J. Raman Spectrosc. 40 (2009) 46–51, https://doi.org/10.1002/jrs.2071.

[38] A.M. Hofmeister, H. -k. Mao, Redefinition of the mode Gruneisen parameter for polyatomic substances and thermodynamic implications, Proc. Natl. Acad. Sci. 99 (2002) 559–564, https://doi.org/10.1073/pnas.241631698.

[39] R.O. Holanda, P.T.C. Freire, J.A.F. Silva, F.E.A. Melo, J.M. Filho, J.A. Lima, High pressure Raman spectra of d-threonine crystal, Vib. Spectrosc. 67 (2013) 1–5, https://doi.org/10.1016/J.VIBSPEC.2013.03.003.

[40] G. Zou, B. Zou, Pressure-induced phase transition in N − H ··· O hydrogen-bonded molecular crystal oxamide, J. Phys. Chem. B 116 (2012) 9796–9802.

[41] T. Yan, D. Xi, Z. Ma, X. Wang, Q. Wang, Q. Li, Pressure-induced phase transition in N–H···O hydrogen-bonded crystalline malonamide, RSC Adv. 7 (2017) 22105–22111, https://doi.org/10.1039/C7RA02205K.

[42] J. Jiang, X. Li, P. Zhu, D. Li, X. Han, Q. Cui, H. Zhu, Effect of pressure on 4-toluenesulfonyl azide studied by Raman scattering and synchrotron X-ray diffraction, J. Phys. Chem. C 121 (2017) 1032–1039, https://doi.org/10.1021/acs.jpcc.6b11016.

[43] S. Klotz, J.-C. Chervin, P. Munsch, G. Le Marchand, Hydrostatic limits of 11 pressure transmitting media, J. Phys. D Appl. Phys. 42 (2009), 075413, https://doi.org/10.1088/0022-3727/42/7/075413.

[44] D. Errandonea, Y. Meng, M. Somayazulu, D. Häusermann, Pressure-induced transition in titanium metal: a systematic study of the effects of uniaxial stress, Phys. B Condens. Matter 355 (2005) 116–125, https://doi.org/10.1016/j.physb.2004.10.030.

[45] M.I. Aroyo, J.M.P. I, C.C. I, E.K. I, S.I. I, G.M. I, Bilbao Crystallographic Server : I . Databases and Crystallographic Computing Programs, vol. 221, 2006, pp. 15–27, https://doi.org/10.1524/zkri.2006.221.1.15.

[46] R.J. Angel, Equations of state, Rev. Miner. Geochem. 41 (2000) 35–59, https://doi.org/10.2138/rmg.2000.41.2.

[47] J. Navarro-Sánchez, I. Mullor-Ruíz, C. Popescu, D. Santamaría-Pérez, A. Segura, D. Errandonea, J. González-Platas, C. Martí-Gastaldo, Peptide metal–organic frameworks under pressure: flexible linkers for cooperative compression, Dalton Trans. 47 (2018) 10654–10659, https://doi.org/10.1039/C8DT01765D.

[48] T.D. Bennett, P. Simoncic, S.A. Moggach, F. Gozzo, P. Macchi, D.A. Keen, J.-C. Tan, A.K. Cheetham, Reversible pressure-induced amorphization of a zeolitic imidazolate framework (ZIF-4), Chem. Commun. 47 (2011) 7983, https://doi.org/10.1039/c1cc11985k.

[49] P. Serra-Crespo, E. Stavitski, F. Kapteijn, J. Gascon, High compressibility of a flexible metal–organic framework, RSC Adv. 2 (2012) 5051, https://doi.org/10.1039/c2ra20528a.

[50] D. Errandonea, R. Boehler, S. Japel, M. Mezouar, L.R. Benedetti, Structural transformation of compressed solid Ar: an x-ray diffraction study to 114 GPa, Phys. Rev. B 73 (2006), 092106, https://doi.org/10.1103/PhysRevB.73.092106.